Synthesis and Characterization of Poly(2-hydroxyethyl methacrylate)-Functionalized Fe-Au/Core-Shell Nanoparticles

Long Giang Bach,[1] Md. Rafiqul Islam,[1] Jin Ho Kim,[1] Hyun Gyu Kim,[2] Kwon Taek Lim[1]

[1]*Department of Imaging System Engineering, Pukyong National University, Busan 608-737, Republic of Korea*
[2]*Busan High Tech Center, Korea Basic Science Institute, Busan 609-735, Korea*

Received 16 July 2011; accepted 25 August 2011
DOI 10.1002/app.35530
Published online 6 December 2011 in Wiley Online Library (wileyonlinelibrary.com).

ABSTRACT: Disulfide-bearing poly(2-hydroxyethyl methacrylate) (DT-PHEMA) was synthesized by atom transfer radical polymerization technique, which was subsequently immobilized onto core-shell structured Fe-Au nanoparticles (Fe-AuNPs) by applying a "*grafting to*" protocol to afford new PHEMA-grafted Fe-AuNPs (PHEMA-*g*-Fe-AuNPs). The Fe-AuNPs having the iron core of 20–22 nm and the gold layer of 1–2 nm were initially prepared by inverse micelle technique and characterized by XRD and high-resolution transmission electron microscopy (HR-TEM). The grafting of DT-PHEMA on the Fe-AuNPs was confirmed by Fourier transformed infrared spectrophotometer, thermogravimetric (TGA), X-ray photoelectron spectroscopy, and energy dispersive X-ray analyses. The average diameter of polymer coated Fe-AuNPs was determined to be 28 nm by HR-TEM analysis. The amount of the polymer on the surface of Fe-AuNPs was calculated to be about 50% by TGA analysis. The studies of magnetic property by the superconducting quantum interference devices indicate the superparamagnetic property of Fe-AuNPs and PHEMA-*g*-Fe-AuNPs. The optical property of the PHEMA-*g*-Fe-AuNPs was recorded by UV–visible absorption spectroscopy, and a redshift in the absorption was observed, which further suggests the PHEMA attachment on the surface of Fe-AuNPs. The magnetic nanocomposites demonstrate good dispersibility in common polar solvents. © 2011 Wiley Periodicals, Inc. J Appl Polym Sci 124: 4755–4764, 2012

Key words: magnetic nanoparticles; iron-gold/core-shell nanoparticles; PHEMA; ATRP; grafting to; hybrid nanocomposites

INTRODUCTION

The emergence of novel materials with intriguing properties and improved performance is a continually expanding research field, which encompasses subjects ranging from chemistry, biology, physics to material science. Polymer-inorganic hybrid nanomaterials are getting rigorous interest because of their fascinating hybrid properties. They integrate the intrinsic properties of inorganic nanostructures with desirable properties of polymers, e.g., processability, solubility, and dispersibility. The incorporation at the nanosize level of active organic and inorganic segments is a critical aspect of current materials science. These functional hybrids are considered as innovative advanced materials with promising applications in many fields such as optics, electronics, sensors, biology, energy storage and conversion, mechanics, catalysis, etc.[1–3]

In the last decade, nanotechnology has matured to such an extent that it is possible to synthesize, characterize, and tailor the functional properties of magnetic nanoparticles for many important application in various areas of biosciences, medicine, material science, and environmental technology.[4–9] Magnetic nanoparticles demonstrate a rich variety of interesting phenomena, such as single-domain state, coercivity enhancement, and quantization of spin wave, due to their small dimensions.[10] In particular, core-shell-structured nanoparticles are of special interest for studying proximity effects and ideal for structure stabilization. Moreover, the shell layer can provide a platform for surface modification to give new functionalization, tuning magnetic properties, and biocompatibility.[11–13] However, the great challenge of their applications in biomedical fields is the poor biocompatibility and the lack of dispersibility in aqueous media. Recently, few efforts have been undertaken to address the prevailing bottlenecks.[14,15]

The coating of magnetic nanoparticles with a suitable noble metal results in air-stable nanoparticles, which protects the core from oxidation and

Correspondence to: K. T. Lim (ktlim@pknu.ac.kr).
Contract grant sponsor: Ministry of Knowledge Economy (MKE) of Korea (Industrial Source Technology Development Program); contract grant number: 10035163.
Contract grant sponsor: MEST (Joint Program of Cooperation in Science and Technology through NRF); contract grant number: 2011-0025680.

corrosion. Gold-coated magnetic nanoparticles have been widely used because of their facile and robust interaction with thiol and disulfide groups that enable them functionalization with various molecules.[16–22] Surface modification with gold also helps to reduce particle agglomeration by steric or electronic repulsion and improves biocompatibility. The unique Au surface is safe for both animals and humans. Thus, magnetic nanocrystals covered with an Au-shell would provide all the characteristics of the Au element suitable for many applications and deliver magnetic properties for further manipulation. Much progress has been made for the functionalization of gold nanoparticles by the use of thiol chemistry, which facilitated the attachment of organic molecules using a variety of thiol linkers.[23–25]

In recent years, an extensive range of new polymeric materials for macromolecular engineering and biological applications by modifying surfaces with polymer brushes has been successfully examined. These are widely used to tailor surface properties such as wettability, biocompatibility, corrosion resistance, and friction.[26,27] In general, there are two basic routes to deposit polymer brushes on the solid surface; one is physical adsorption and the other is covalently attachment by a chemical reaction. Covalently bonded polymers can usually overcome drawbacks of that prepared by physical adsorption, such as low grafting densities and adhesive force. At present, widely used polymerization technique for the growth of polymer brushes from surfaces are controlled/"living" radical polymerization methods, such as nitroxide-mediated radical polymerization, reversible addition fragmentation chain transfer polymerization, and atom transfer radical polymerization (ATRP).[28–31] Among these methods, ATRP has been used successfully to coat both organic and inorganic nanoparticles with different types of polymers. In addition, *grafting to* and *grafting from* approaches are the most common methods to synthesis covalently attached polymer brushes at a surface.[32–34] Although grafting-from strategy can be well controlled leading to achieve high grafting density but it requires additional surface functionalization for polymerization. In contrast, grafting to approach is experimentally simple. In some biomedical applications, it is desirable to functionalize magnetic nanoparticles with polymer shells bearing specific functional groups capable of conjugation or immobilization of foreign biological molecules.[35,36] The hydroxyethyl moieties of poly (2-hydroxyethyl methacrylate) (PHEMA) confer high hydrophilicity on the polymer. It is widely used in biotechnological and biomedical applications to prepare various hydrogels, immobilize proteins or cells, etc.[37–39]

Albeit abundant reports related to functionalization of magnetic nanoparticles (MNPs) exist,[28—31] the number of studies addressing the surface functionalization of gold-coated iron MNPs by polymers is very limited. Triblock copolymer-coated Fe-Au nanoparticles were reported by Wu and coworkers,[12] where they prepared the nanoparticles through a nanoemulsion method by mixing iron salt, gold salt, and the surfactant (PEO-PPO-PEO) together at an elevated temperature. Another report on the anchoring of Fe-Au nanoparticles with polyglycerol-grafted graphene oxide has recently disclosed, in which functionalization of nanoparticles was accomplished.[24] By taking the aforesaid observations into account, we were interested to develop a facile method for surface functionalization of MNPs with a biocompatible PHEMA on covalent immobilization.

In this study, we demonstrate a facile synthesis of covalently immobilized biocompatible PHEMA onto the surface of gold-layered Fe-nanoparticles. The fabrication of gold-coated iron nanoparticles (Fe-AuNPs) were initially accomplished by using a two-step reverse micelle process. Disulfide-containing PHEMA was synthesized under ATRP using 2-(2′-bromoisobutyroyloxy)ethyl disulfide (DT-Br) as an initiator, which subsequently anchored to the Fe-AuNPs. The characterization and properties of the magnetic nanocomposites (MNCs) were fully accomplished by spectroscopic as well as all other relevant analyses. So far, it is the first example of PHEMA-functionalized MNPs by a grafting to protocol to the best of our knowledge.

EXPERIMENTAL

Materials

Cetyltrimethylammonium bromide (CTAB) ($C_{19}H_{42}BrN$), iron (II) sulfate heptahydrate ($FeSO_4.7H_2O$), hydrogen tetrachloroaurate (gold solution; 30 wt % in dilute HCl), sodium borohydride ($NaBH_4$), octane, *n*-butanol, 2,2′-dithiodiethanol, ethyl 2-bromoisobutyrate (99%), copper(I) chloride (CuCl, 99.99%), and 2,2′-bipyridine (bipy) were purchased from Sigma–Aldrich (Yongin, Korea). 2-Hydroxyethyl methacrylate (HEMA) was passed through a 10-cm column of basic alumina to remove inhibitors. Chloroform, methyl ethyl ketone (MEK), and 1-propanol were dried over CaH_2 and distilled before use.

Synthesis of Fe-AuNPs by a reverse micelle method

Fe-AuNPs were prepared using a reverse micelle method, which is also called the water-in-oil microemulsion method.[19] The synthesis was carried out under the flow of argon gas in a glove box. Reverse micelle solutions were prepared using CTAB as a surfactant, octane as a oil phase, and 1-butanol as a

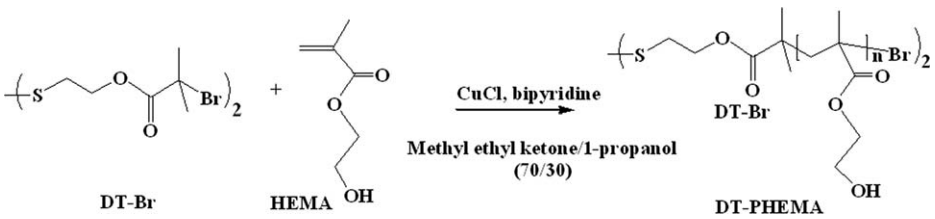

Scheme 1 Preparation of DT-PHEMA by ATRP using DT-Br.

cosurfactant. The water droplet size of the reverse micelles was controlled by the molar ratio of water to the surfactant. In the first step, Fe nanoparticles were obtained by the reduction of $FeSO_4$ with $NaBH_4$. In a typical experiment, 0.36 g (2.4 mmol) of $FeSO_4$ was added to the inverse micelle solution and then 0.18 g (4.8 mmol) of $NaBH_4$ was added to the solution by using a double-ended needle. This mixture was stirred at room temperature under argon atmosphere. The solution turned green and then black, indicating the formation of iron nanoparticles. In the second step, gold shells were formed by reducing $HAuCl_4$. On stirring, the micelle solution of $HAuCl_4$ (0.27 g, 0.8 mmol) was prepared and added to the earlier prepared black solution (i.e., mixture of $FeSO_4$ and $NaBH_4$). A micelle solution of 0.11 g (2.9 mmol) of $NaBH_4$ was immediately added to the solution. The mixture was left stirring at room temperature overnight. Finally, dark precipitates were collected by using a strong permanent magnet and washed with a mixture of chloroform and methanol for several times to remove residual nonmagnetic particles and organic surfactants. The product Fe-AuNPs was then dried overnight in a vacuum oven.

Synthesis of disulfide-carrying ATRP initiator (DT-Br)

2-Bromoisobutyryl bromide (6.60 g, 5.34×10^{-2} mol) was added dropwise to a stirred solution of 2,2′-dithiodiethanol (3.40 g, 2.21×10^{-2} mol) and pyridine (4.30 g, 5.32×10^{-2} mol) in dry chloroform (60 mL) at 0°C under argon atmosphere.[35] The solution mixture was stirred at 0°C for 1 h and then at room temperature for 24 h. After completion of the reaction, the solvent was removed by a rotary vacuum evaporator under reduced pressure. The oily mixture was dissolved in ether and washed with a saturated aqueous ammonium chloride solution. After drying over Na_2SO_4, the solvent was removed under reduced pressure. The product, DT-Br, was purified by silica gel column chromatography (mobile phase, ethyl acetate/hexane = 1 : 4). The resulting product DT-Br is colorless oil (7.816 g, 78.2% yield).^{1}H-NMR (400 MHz, $CDCl_3$): δ 4.39 (t, 4H, OCH_2), 2.93 (t, 4H, SCH_2), 1.89 (s, 12H, CH_3); ^{13}C-NMR ($CDCl_3$): δ 171.46 (C=OO), 63.41 (OCH_2), 55.43 (C—Br), 36.63 (S—CH_2), 30.62 (CH_3).

Preparation of disulfide-carrying PHEMA by ATRP technique

In a typical ATRP procedure (Scheme 1), HEMA (1.30 g, 1×10^{-2} mol) and a mixture of MEK and 1-propanol (70 : 30) (2.6 mL) were taken in a dry 100-mL Schlenk flask. The tube was sealed with a rubber septum and subjected to three freeze-pump-thaw cycles, then the solution was cannulated under argon into another Schlenk tube which was previously evacuated containing DT-Br initiator (45.2 mg, 1×10^{-4} mol), Cu(I)Cl (9.95 mg, 1×10^{-4} mol), bpy (46.8 mg, 3×10^{-4} mol), and a Teflon-coated magnetic spin bar. A predegassed reflux condenser with gas inlet/outlet was attached to the flask quickly, and the system was purged with argon. The ampoules were immediately placed in a thermostatic oil bath at 70°C. The reaction mixture became immediately dark brown and progressively more viscous, indicating the onset of polymerization. After 12 h of reaction, the reaction mixture was cooled to room temperature, and the product was passed through a short column filled with activated alumina to remove the ATRP catalyst. Afterward, the eluent was eliminated by a rotary evaporator. The solution was precipitated in a large excess of diethyl ether. Finally, the polymers were dried under vacuum until reaching constant weight. A polymer yield was determined gravimetrically.

Grafting of DT-PHEMA onto Fe-AuNPs

A schematic representation of the surface functionalization of Fe-AuNPs with disulfide-bearing poly (2-hydroxyethyl methacrylate) (DT-PHEMA) is shown in Scheme 2. In a typical procedure, 0.1 g of DT-PHEMA was mixed with 0.1 g of Fe-AuNPs in 50 mL of methanol. After vigorous stirring for 12 h at room temperature, the solvent was removed by reduced pressure-distillation without exceeding the temperature of 50°C. Then, the dark residue was washed thoroughly with methanol to remove excess DT-PHEMA. Finally, the material was dried in a vacuum oven at

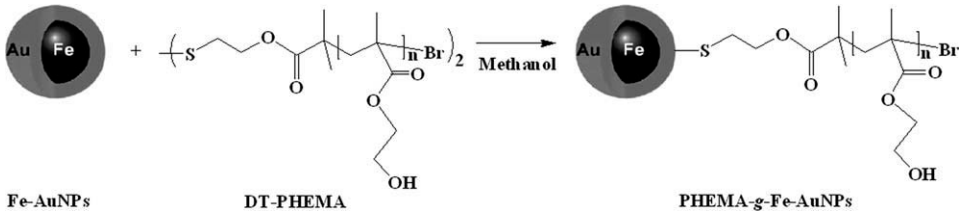

Scheme 2 Synthesis of PHEMA-*g*-Fe-AuNPs.

45°C to obtain the PHEMA-grafted Fe-AuNPs (PHEMA-*g*-Fe-AuNPs) as dark-brown powder.

Characterization and measurements

High-resolution transmission electron microscopy (HR-TEM) images were recorded using a Joel JEM 2010 instrument (Japan) with an accelerating voltage of 200 kV. A drop of the sample dispersed in distilled water was placed on a copper grid for the analysis. The changes in the surface chemical bonding of functionalized Fe-AuNPs were captured by Fourier transformed infrared spectrophotometry (FTIR) using a BOMEM Hartman and Braun FTIR spectrometer in the frequency range of 4000–400 cm^{-1}. The absorption spectra of the nanocomposites dispersed in ethanol were obtained using Perkin–Elmer Lambda 40 Ultraviolet–visible spectrophotometer. The elemental analysis of the hybrids was carried out by using a Field-emission scanning electron microscopy equipped with an energy dispersive X-ray (EDX) spectrometer (HitachiJEOL-JSM-6700F system, Japan). Thermogravimetric analysis (TGA) was conducted with a Perkin–Elmer Pyris 1 analyzer. Before the test, all the samples were carefully grinded into fine powder. The samples were scanned within the temperature range of 50–700°C at a heating rate of 10°C min^{-1} under continuous nitrogen flow. Surface composition was investigated using a X-ray photoelectron spectroscopy (XPS; Thermo VG Multilab 2000) in ultrahigh vacuum with Al Kα radiation. The crystallographic state of Fe-AuNPs was determined by a Philips X'pert-MPD system diffractometer (Netherlands) with Cu Kα radiation. Magnetic measurements were performed at 300°K using a superconducting quantum interference device magnetometer (SQUID) (Quantum design MPMS-XL7). Gel permeation chromatography (GPC) analyses of the samples were carried out on an Agilent 1200 Series equipped with PLgel 5 μm MIXED-C columns, with *N*,*N*-dimethylformamide as the solvent at 30°C. The solution flow rate was 1 mL min^{-1}. Calibration was carried out using polymethylmethacrylate (PMMA) standards.

The ^{1}H-NMR spectrum of DT-Br and DT-PHEMA were recorded using a JNM-ECP 400 (JEOL) spectrophotometer with solvents $CDCl_3$ and CD_3OD, respectively.

RESULTS AND DISCUSSION

Characterization of the Fe-AuNPs by XRD and HR-TEM

The X-ray Diffraction (XRD) pattern of the crystalline structure of the Fe-AuNPs is shown in Figure 1. As seen in the trace, the peaks at 38.14°, 44.36°, and 64.58° are assigned to face centered cubic (fcc) bulk gold of (1 1 1), (2 0 0), and (2 2 0). The pattern (1 1 0) and (2 0 0) of iron peaks are overlapped with (2 0 0) and (2 2 0) of gold peaks at 44.36° and 64.58°, indicating the complementary growth of gold shells on the iron cores.[19] In addition, no iron oxide peak was detected with considering the technical detection limit of the X-ray method. This unequivocally indicates that the iron core was protected by the gold shell from oxidation.

Figure 2 shows the morphology and particle sizes of the Fe-AuNPs. The core-shell structure of the Fe-AuNPs can easily be observed in Figure 2(a,b), where the formation of gold shell layers as bright regions on the surface of the iron cores is clearly visualized. The higher magnification TEM image of a single Fe-Au nanoparticle is shown in Figure 2(c), where it is observed that the fringe lattices run almost uniformly over the whole nanoparticle. The spacing of the lattices is 2.0 Å, corresponding to the (200) reflection of the Fe-Au fcc phase.[19] The average size of the nanoparticles was found to be about 21–24 nm. TEM studies revealed that the thickness of

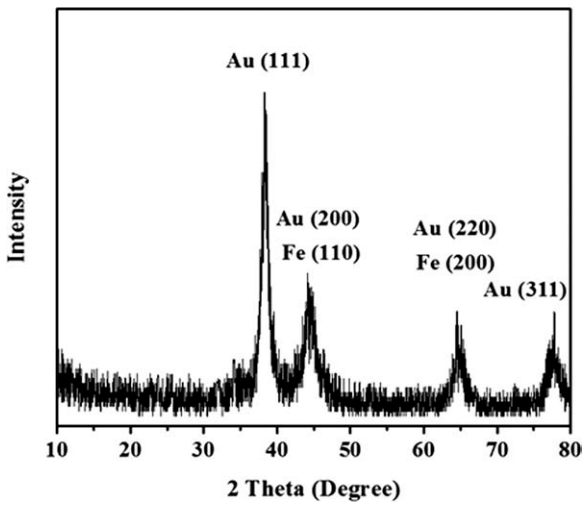

Figure 1 XRD patterns of the Fe-AuNPs.

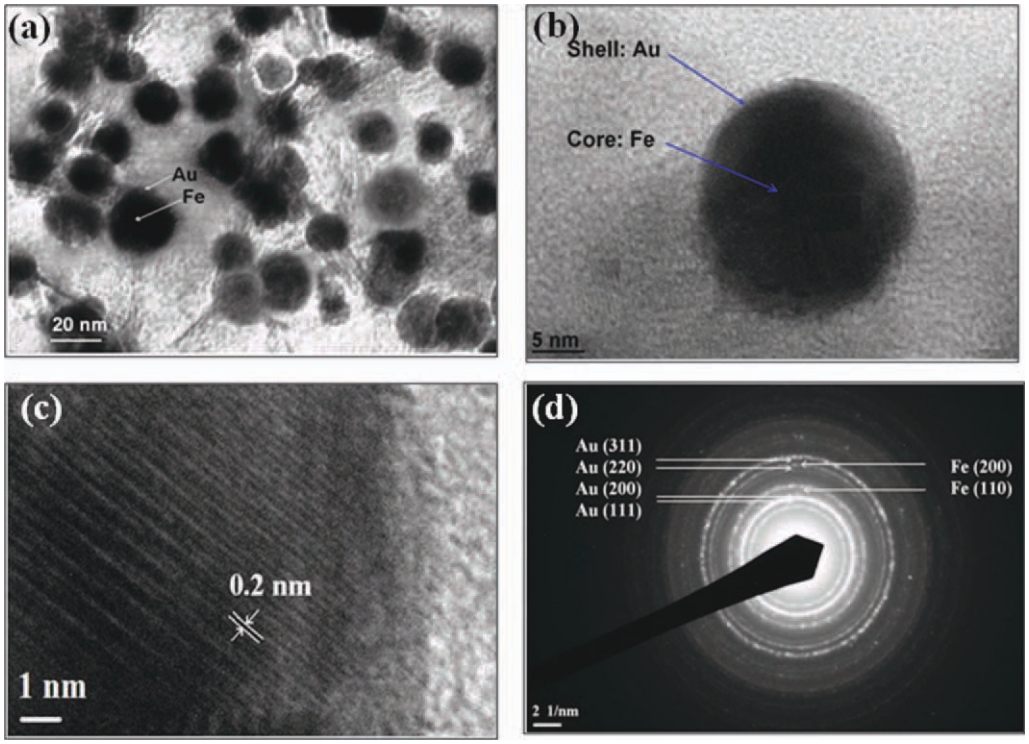

Figure 2 The TEM images of (a) Fe-AuNPs, (b) and (c) a single Fe-AuNP, (d) diffraction pattern of a single Fe-AuNPs. [Color figure can be viewed in the online issue, which is available at wileyonlinelibrary.com.]

the gold layer ranged from 1 to 2 nm, and the size of the iron core was about 20–22 nm. The selected area of electron diffraction pattern of the Fe-AuNPs obtained from TEM micrograph is depicted in Figure 2(d). In the diffraction patterns, the presence of both gold and iron in a single particle is observed, and it is seen that peaks (200), (220), and (222) assigned for gold overlaps with the peaks ascribed for iron (110), (200), and (211).[16]

Characterization of DT-PHEMA by ^{1}H-NMR and GPC

DT-PHEMA was synthesized easily by ATRP of HEMA using the difunctionalized initiator DT-Br having a disulfide group as shown in Scheme 1. In this system, HEMA was polymerized in a mixture of MEK and 1-propanol (70 : 30) at 70°C with an initial molar ratio of [HEMA] : [DT-Br] : [Cu(I)Cl] : [bpy] = 100 : 1 : 1 : 3. The chemical structure of the DT-PHEMA was confirmed by ^{1}H-NMR spectroscopy, and the spectrum is shown in Figure 3. The ^{1}H-NMR spectrum demonstrates two broad peaks at the range of 0.90–1.18 ppm which are ascribed for methyl protons (a, a′) and a broad peak assign for hydroxyl proton (c) at 2.01–2.10 ppm. The peaks at 1.94, 3.76, and 4.02 ppm could be ascribed for the methylene protons of (b), (e), and (f), respectively, which are positioned on the backbone of the polymer. The remaining two peaks on the spectrum at 2.98 and 4.19 ppm should be assigned for (d) methylene protons (—CH_2—S) and (g) methylene protons (—CH_2—O), respectively. The NMR data suggest that the ATRP reaction effectively occurred in the solution.

The molecular weights and molecular weight distribution of the DT-PHEMA were analyzed by GPC to give the weight average molecular weight of 9.6 kg mol^{-1} and PDI (M_w/M_n) of 1.40. The typical GPC curve of DT-PHEMA is presented in Figure 4.

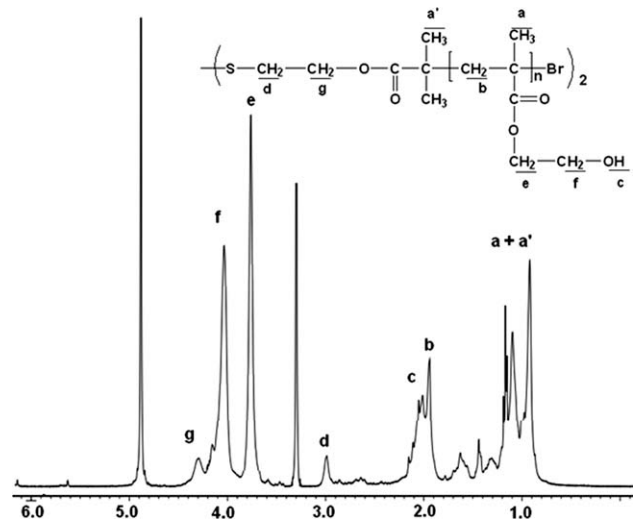

Figure 3 ^{1}H-NMR spectrum of the DT-PHEMA in CD3OD.

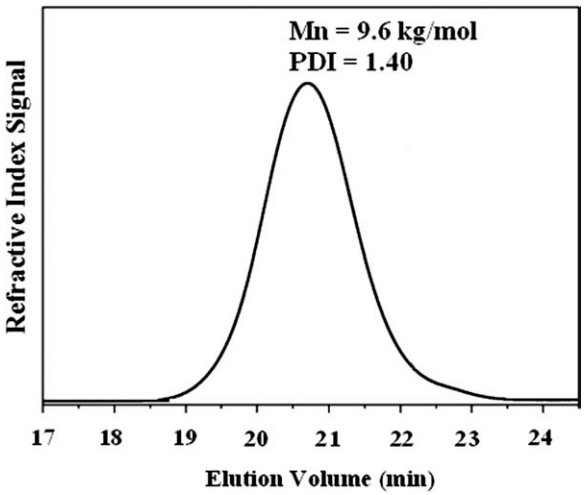

Figure 4 GPC trace of DT-PHEMA.

The narrow GPC curve indicates that the ATRP polymerization process was performed in a controlled manner.

Characterization of PHEMA-*g*-Fe-AuNPs by FTIR, XPS, EDX, TEM and TGA

The grafting of DT-PHEMA on the surface of the Fe-AuNPs was analyzed by FTIR spectroscopy. The FTIR spectra of the Fe-AuNPs, DT-PHEMA, and PHEMA-*g*-Fe-AuNPs are shown in Figure 5. In the case of Fe-AuNPs [Fig. 5(a)], characteristics bands at 3376 cm^{-1} (H—O stretching) and 1630 cm^{-1} (H—O—H bending) are due to adsorbed water on the surface of the nanoparticles, and the band at 1390 cm^{-1} (C—C stretching) arises from the CTAB surfactant.[20] The FTIR spectrum of DT-PHEMA shows multiple bands at 3450 (O—H stretching) and 1728 cm^{-1} (—C=O stretching). The bands in the range of 2700–2950 cm^{-1} can be interpreted for C—H stretching for methyl —CH_3 and methylene —CH_2— groups, and also the band at 1450 cm^{-1} is ascribed for —C—H bending. The band at 732 cm^{-1} represents —CH_2—S, and the bands at 564 and 486 cm^{-1} might indicate S—S stretching. The characteristic FTIR spectrum of the DT-PHEMA grafted onto the surface of Fe-AuNPs is depicted in Figure 5(c). In comparison with the FTIR spectrum of the sole Fe-AuNPs, the DT-PHEMA-*g*-Fe-AuNPs spectrum shows a strong absorption peak at 1730 cm^{-1}, which is assigned to the ester carbonyl (C=O) associated with PHEMA units. The spectrum also shows two characteristic absorptions at 2930 and 1156 cm^{-1}, which are attributed to the stretching vibrations of C—H and C—O—C, respectively. The changes in the band shape of the carbonyl stretching and C—H bending might involve the coordination of the oxygen atoms in the main chains on the Au metallic atoms.[12] In addition, the characteristic absorption at the range of 3300–3500 cm^{-1} could assign to the hydroxyl groups which becomes broader and stronger as the HEMA units were introduced on the Fe-AuNPs surface. Noticeably, the band shape and absorption intensities differ considerably among the Fe-AuNPs, DT-PHEMA, and PHEMA-*g*-Fe-AuNPs. The FTIR results have provided useful evidences that PHEMA was successfully grafted onto the Fe-AuNPs.

In addition to FTIR, XPS analysis was used to confirm and determine the composition of PHEMA-*g*-Fe-AuNPs. The XPS spectrum indicates that the sample PHEMA-*g*-Fe-AuNPs is composed of Fe, Au, C, S, Br, and O as shown in Figure 6. Fe2p electrons show binding energy (BE) at 711 and 725 eV, while the BE of Au4f electrons is seen at 87.0 and 83.2 eV, indicating the presence of iron and gold in the sample. The major peak component at the BE of about 285.10 eV is assigned to the C1s, the strongest peak at 532.7 eV corresponds to the O1s, and the peak observed at 163.2 eV corresponds to the S2p of the thiol functional groups on Fe-AuNPs. The BE of Br3d electrons is found at 69.2 eV. Hence, all of these results strongly suggest that the grafting of PHEMA was successfully achieved onto the surface of Fe-AuNPs through sulfide linkages.

The components of the PHEMA-*g*-Fe-AuNPs were examined by EDX, and the elemental mapping analysis is shown in Figure 7. The characteristic peaks ascribed for gold, iron, carbon, oxygen, sulfur, and bromine elements are present in the EDX spectrum of PHEMA-*g*-Fe-AuNPs, which unanimously interprets that PHEMA is immobilized onto the surface of Fe-AuNPs.

The morphology and particle size of the PHEMA-*g*-Fe-AuNPs were recorded by TEM (Fig. 8). As seen

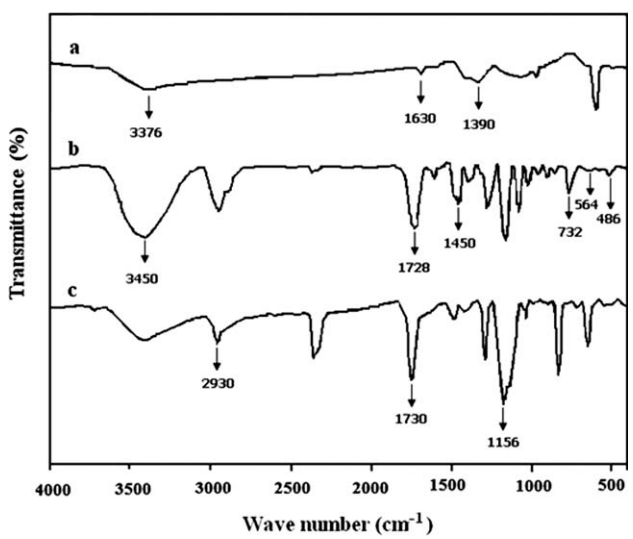

Figure 5 FTIR spectra of (a) Fe-AuNPs, (b) DT-PHEMA (c) PHEMA-*g*-Fe-AuNPs.

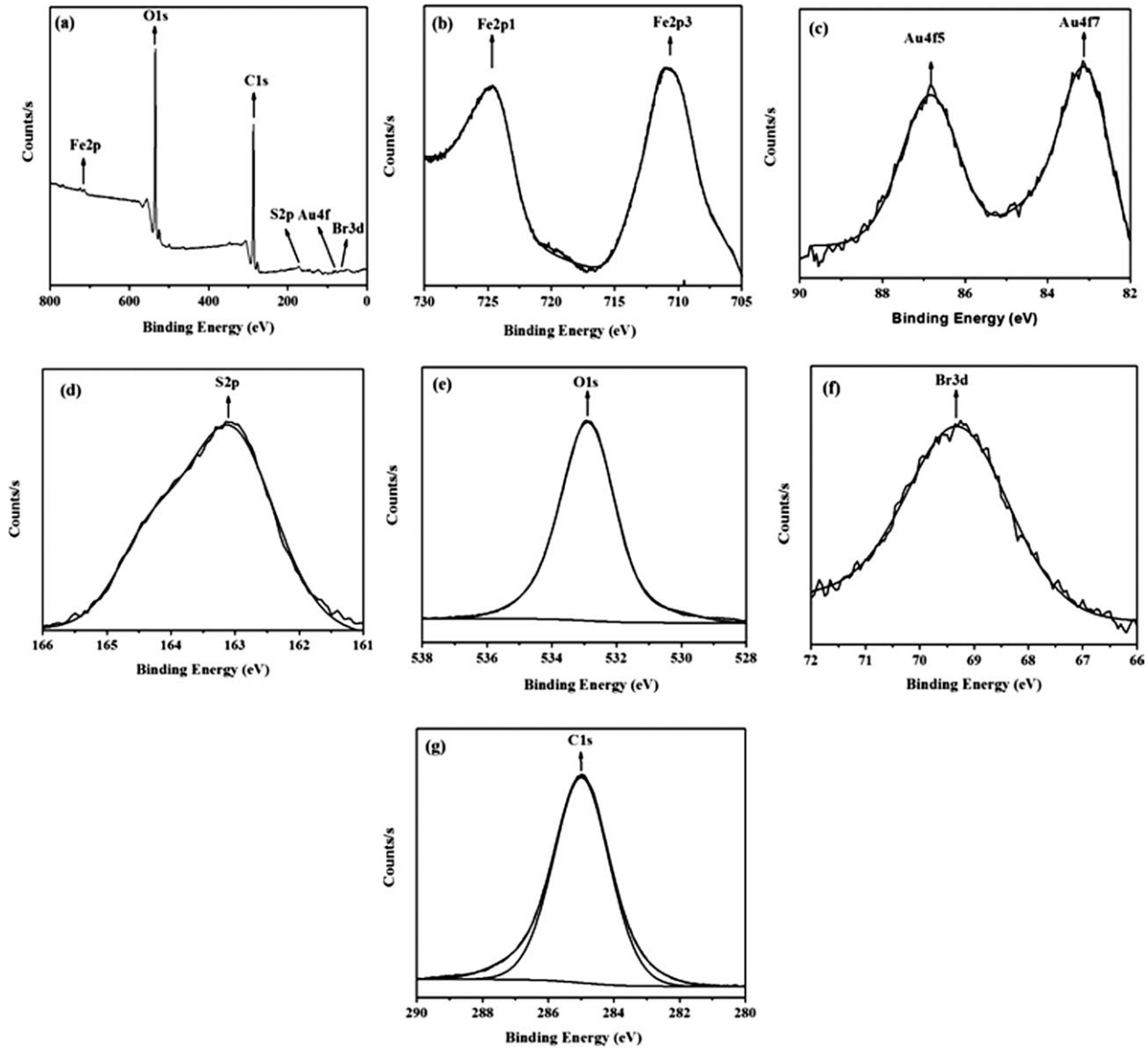

Figure 6 XPS spectra of PHEMA-*g*-Fe-AuNPs: (a) full XPS spectrum of a typical sample, (b) Fe2p, (c) Au4f, (d) S2p, (e) O1s, (f) Br3d, (g) C1s core-level spectra of the functionalized PHEMA-*g*-Fe-AuNPs surfaces.

in Figure 8(a), the nanocomposites are almost uniform and spherical in shape, comparable to the Fe-AuNPs [Fig. 2(b)]. In Figure 8, the light contrast shell is ascribed for PHEMA, whereas the dark contrast core is assigned for Fe-AuNPs. The Figure 8(b) shows the enlarged view of a portion of the TEM image, illustrating more clearly that the Fe-AuNPs were coated with a uniform and well-defined dense polymer layer. The size distribution of the nanoparticles gives an average particle size of 28 nm in diameter. As compared with the Fe-AuNPs, the samples PHEMA-*g*-Fe-AuNPs still remained monodisperse, and an increase in the average diameter is $\sim$ 4–6 nm.

To examine the composition effect on the thermal degradation of PHEMA-*g*-Fe-AuNPs, TGA analyses were performed for all the samples at the

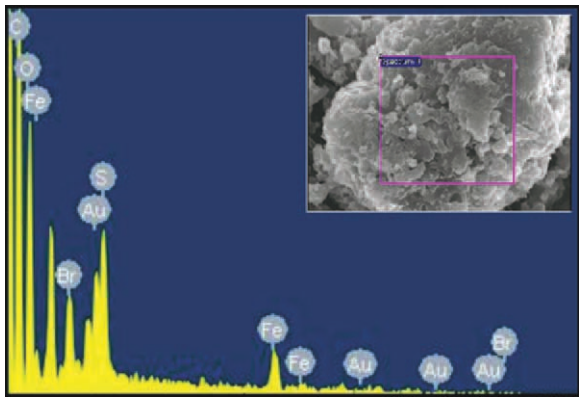

Figure 7 EDX analysis of PHEMA-*g*-Fe-AuNPs. [Color figure can be viewed in the online issue, which is available at wileyonlinelibrary.com.]

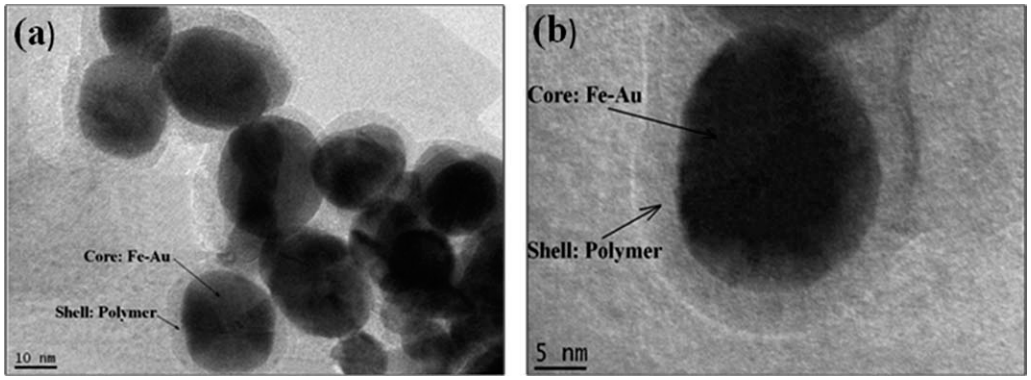

Figure 8 TEM images of PHEMA-*g*-Fe-AuNPs: (a) a microgram of a typical sample, (b) an enlarged view of a portion of the TEM image.

temperature range from 50 to 700°C. TGA curves of Fe-AuNPs, DT-PHEMA, and PHEMA-*g*-Fe-AuNPs are shown in Figure 9, from which the initial degradation temperature and final degradation temperature were determined. In Figure 9(a), it is seen that the sample of Fe-AuNPs lose 8% of their total weight, which could be due to the decomposition of CTAB surfactant present in the sample because it was not removed completely by the washing process.[24] The weight loss curve of DT-PHEMA indicates that initial degradation starts at 322°C and reaches maximum at 450°C [Fig. 9(c)]. In comparison with Fe-AuNPs, the TGA curve of PHEMA-*g*-Fe-AuNPs showed that a major decomposition occurred at the temperature range from 250 to 420°C, which corresponds to the surface-grafted PHEMA on Fe-AuNPs [Fig. 9(b)]. The amount of the polymer on the surface of Fe-AuNPs is calculated about 50%, which suggests that a moderate degree of functionalization of PHEMA on the surface of the Fe-AuNPs was achieved by the grafting to method.

Optical and magnetic properties of PHEMA-grafted Fe-AuNPs

The effect of PHEMA grafting onto Fe-AuNPs was further investigated by measuring the optical properties of the nanoparticles because of surface plasmons ensuing from the nanostructured Au. The UV–vis spectra for pure Au nanoparticles, Fe-AuNPs, DT-PHEMA, and PHEMA-*g*-Fe-AuNPs are shown in Figure 10. The UV–vis spectra of Au and Fe-AuNPs exhibit a surface plasmon resonance and a maximum absorption band observe at 521 and 554 nm as shown in Figure 10(a,b). The absorption is in good agreement with the reported observation which gives the complementary color of the absorption. Evidently, the solution of the PHEMA-*g*-Fe-AuNPs shows a broadband absorption shape with the maximum absorption at 582 nm [Fig. 10(c)], suggesting the evidence of the optical property of Fe-AuNPs. In the UV–vis spectrum, it is seen that both Au and Fe-AuNPs show relatively narrow band shapes, while PHEMA-*g*-Fe-AuNPs shows

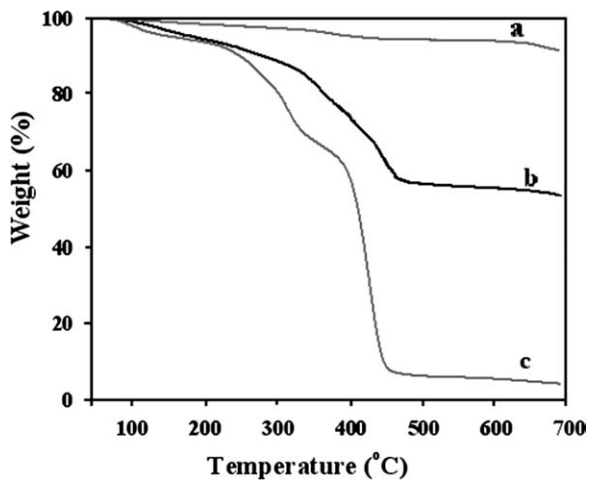

Figure 9 TGA thermograms of (a) Fe-AuNPs, (b) PHEMA-*g*-Fe-AuNPs, (c) DT-PHEMA.

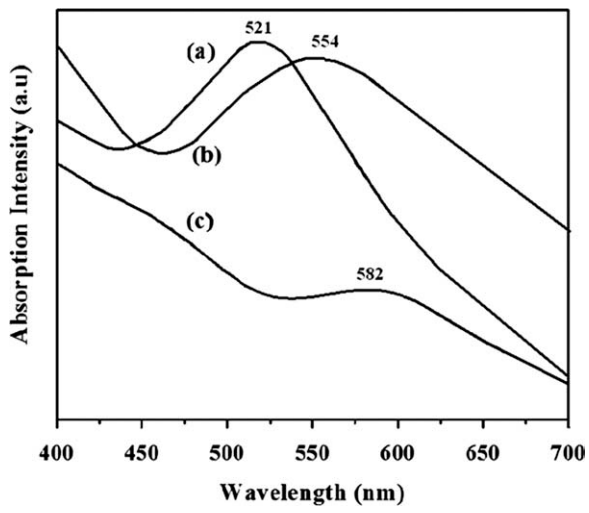

Figure 10 UV–vis absorption spectra of (a) Au nanoparticles, (b) Fe-AuNPs, (c) PHEMA-*g*-Fe-AuNPs.

reasonably the higher band shape. The UV–vis spectrum of PHEMA-*g*-Fe-Au NPs shows a broadband shape that might be due to the interaction of DT-PHEMA with gold surface. This interaction is presumably because of the attachment of DT-PHEMA with gold arising from the strong electrostatic attraction of active group (disulfides) in DT-PHEMA with gold layer on Fe-Au-NPs.

To study the magnetic property of the Fe-AuNPs, magnetization measurements were carried out by SQUID. The magnetization curves of the samples before and after grafting PHEMA on Fe-AuNPs are demonstrated in Figure 11. The hysteresis curve was not observed at the low magnetic filed at room temperature. As expected, the saturation magnetization values for the PHEMA-*g*-Fe-AuNPs (14.1 emu g^{-1}) is less than that of both Fe-NPs (32.3 emu g^{-1}) and Fe-AuNPs (22.6 emu g^{-1}), which might be because of the presence of PHEMA polymer on the surface of Fe-AuNPs. The adsorbed polymer on the surface of Fe-AuNPs changes the surface magnetic anisotropy, which causes the increase of the surface spins disorientation. The magnetizations versus applied magnetic field (M–H loop) curves of Fe-AuNPs and PHEMA-*g*-Fe-AuNPs show zero coercivity and remanence, which clearly suggests their superparamagnetic behavior. The observation is fully consistent with reported results.[18]

Dispersion stability of the PHEMA-grafted Fe-AuNPs

To study the dispersion behavior of the synthesized Fe-AuNPs, two separate suspensions of Fe-AuNPs and PHEMA-*g*-Fe-AuNPs were prepared in methanol. When Fe-AuNPs were taken into either water or methanol and the solution was subjected to sonication for long time, a true dispersion was not

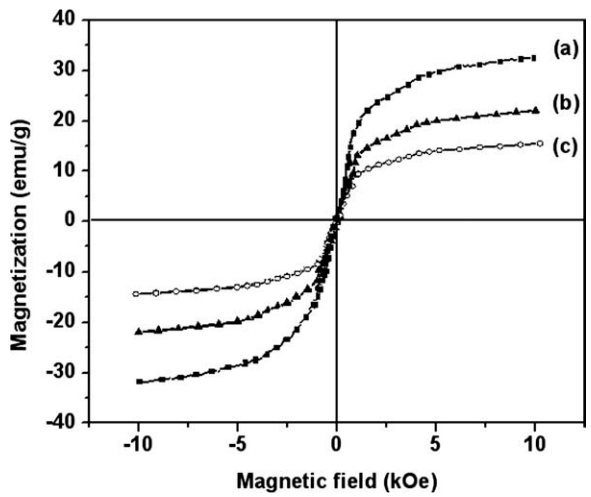

Figure 11 Magnetization curves of (a) Fe-NPs, (b) Fe-AuNPs, (c) PHEMA-*g*-Fe-AuNPs at room temperature.

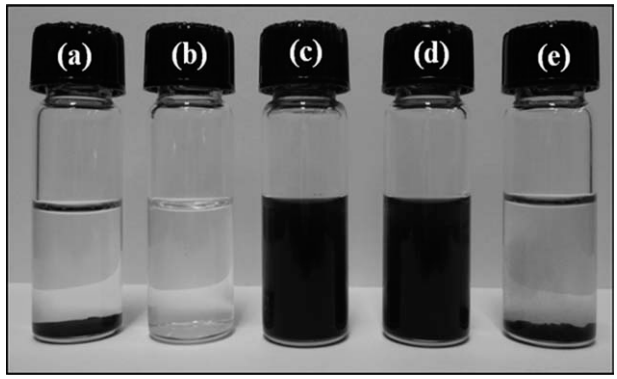

Figure 12 Dispersibility of (a) Fe-AuNPs, (b) DT-PHEMA, (c) PHEMA-*g*-Fe-AuNPs dispersed in water, (d) PHEMA-*g*-Fe-AuNPs dispersed in methanol, (e) PHEMA with Fe-nanoparticles in water (1.0 wt %).

observed, besides the sedimentation of Fe-AuNPs was visualized [Fig. 12(a)]. When DT-PHEMA was suspended in either water or methanol, a clear dispersion was formed as shown in Figure 12(b). However, the clear dispersion of PHEMA-*g*-Fe-AuNPs in either water or methanol could easily be prepared as shown in the digital photograph [Fig. 12(c,d)]. The resulting solutions of the MNCs dispersed in water and methanol have good stability up to a week most presumably due to the attachment of DT-PHEMA to the Fe-AuNPs via Au-S linkage. A control experiment was conducted whether iron surface is prone to functionalize by DT-PHEMA, under the similar condition. In this regard, Fe nanoparticles were prepared by the reduction of $FeSO_4$ with $NaBH_4$, and then the grafting effort of PHEMA on the Fe nanoparticles was undertaken by using DT-PHEMA under the similar reaction condition as mentioned in Scheme 2. The resulting crude mixture was taken in distilled water and subjected to sonication for long time. However, the photograph of the sonicated mixture showed that the Fe nanoparticles completely came out form the suspension giving black sedimentation [Fig. 12(e)]. This result demonstrates that the surface of Fe-nanoparticles is not prone for functionalization by DT-PHEMA in contrast with Fe-AuNPs, which indicates that the Au-shell is playing a significant role for this functionalization.

CONCLUSIONS

PHEMA-grafted hybrid MNCs (PHEMA-*g*-Fe-AuNPs) were successfully synthesized in a facile manner. Initially, Fe-AuNPs were prepared by a reverse micelle method, which had the Fe cores with the size of 20–22 nm and thin gold shell layers of about 1–2 nm thicknesses. DT-PHEMA was prepared with the disulfide-carrying initiator DT-Br and subsequently used to functionalize the surface of the Fe-AuNPs by the interaction of disulfide moieties with Au. The grafting of Fe-AuNPs with

DT-PHEMA was unequivocally confirmed by spectroscopic (NMR, FTIR, XPS, and EDX) as well as other relevant (TEM and TGA) analyses. The TEM image revealed that uniform and well-defined polymer-coated Fe-AuNPs with an average diameter of 28 nm were afforded after the functionalization of PHEMA. The moderate degree of functionalization on the surface of the Fe-AuNPs (ca. 50%) was observed from TGA. The UV–vis spectra demonstrated that PHEMA coated Fe-AuNPs (χ_{max} 582 nm) displayed reasonably higher band shape than that of the uncoated Fe-AuNPs (χ_{max} 554 nm). The magnetization curves of Fe-AuNPs and PHEMA-*g*-Fe-AuNPs showed zero coercivity and remanence, indicating their superparamagnetic property. The nanocomposites exhibited excellent dispersibility in polar solvents such as water and methanol thanks to the surface PHEMA chains. It is highly expected that the biocompatible PHEMA-*g*-Fe-AuNPs nanocomposites would be promising compounds in material science especially in biotechnological and biomedical applications.

References

1. Alivisatos, P. Science 1996, 271, 933.
2. Kim, G. M.; Wutzler, A.; Radusch, H. J.; Michler, G. H.; Simon, P.; Sperling, R. A.; Parak, W. J Chem Mater 2005, 17, 4949.
3. Song, S. H.; Jeong, H. K.; Kang, Y. G. J Ind Eng Chem 2010, 16, 1059.
4. Kim, J.; Piao, Y.; Hyeon, T. Chem Soc Rev 2009, 38, 372.
5. Chu, M.; Song, X.; Cheng, D.; Liu, S.; Zhu, J. Nanotechnology 2006, 17, 3268.
6. Shinkai, M. J Biosci Bioeng 2002, 94, 606.
7. Corot, C.; Robert, P.; Idée, J. M.; Port, M. Adv Drug Deliv Rev 2006, 58, 1471.
8. Safarik, I.; Safarikova, M. Solid State Phenom 2009, 151, 88.
9. Hao, R.; Xing, R.; Xu, Z.; Hou, Y.; Gao, S.; Sun, S. Adv Mater 2010, 22, 2729.
10. Martin, J. I.; Nogues, J.; Liu, K.; Vicente, J. L.; Schuller, I. K. J Magn Magn Mater 2003, 256, 449.
11. Kayal, S.; Ramanujan, R. V. Mat Sci Eng C 2010, 30, 484.
12. Liu, H. L.; Hou, P.; Zhang, W. X.; Kim, Y. K.; Wu, J. H. Nanotechnology 2010, 21, 335602.
13. Lei, Z.; Li, Y.; Wei, X. J Solid State Chem 2008, 181, 480.
14. Zhang, M.; Cushing, B. L.; O'Connor, C. J. Nanotechnology 2008, 19, 085601.
15. Park, H. Y.; Schadt, M. J.; Wang, L.; Lim, I. S.; Njoki, P. N.; Kim, S. H.; Jang, M. Y.; Luo, J.;.Zhong, C. J. Langmuir 2007, 23, 9050.
16. Cho, S. J.; Kauzlarich, S. M.; Olamit, J.; Liu, K.; Grandjean, F.; Rebbouh, L.; Long, G. J. J Appl Phys 2004, 95, 6804.
17. Rudakovskaya, P. G.; Beloglazkina, E. K.; Majouga, A. G.; Zyk, N. V. Mendeleev Commun 2010, 20, 158.
18. Lin, J.; Zhou, W.; Kumbhar, A.; Wiemann, J.; Fang, J.; Carpenter, E. E.; O'Connor, C. J. J Solid State Chem 2001, 159, 26.
19. Carpenter, E. E.; Kumbhar, A.; Wiemann, J. A.; Srikanth, H.; Wiggins, J.; Zhou, W.; O'Connor, C. J Mater Sci Eng A 2000, 286, 81.
20. Kayal, S.; Ramanujan, R. V. J Nanosci Nanotechnol 2010, 10, 1.
21. Bai, Y.; Teng, B.; Chen, S.; Chang, Y.; Li, Z. Macromol Rapid Commun 2006, 27, 2107.
22. Jafari, T.; Simchi, A.; Khakpash, N. J Colloid Interface Sci 2010, 345, 64.
23. Zhu, M.; Aikens, C. M.; Hollander, F. J.; Schatz, G. C.; Jin, R. J Am Chem Soc 2008, 130, 5883.
24. Pham, T. A.; Kumar, N. A.; Jeong, Y. T. Synth Met 2010, 160, 2028.
25. Daniel, M. C.; Astruc, D. Chem Rev 2004, 104, 293.
26. Braunecker, W. A.; Matyjaszewski, K. Prog Polym Sci 2007, 32, 93.
27. Barbey, R.; Lavanant, L.; Paripovic, D.; Schúwer, N.; Sugnaux, C.; Tugulu, S.; Klok, H. A. Chem Rev 2009, 109, 5437.
28. Matsuno, R.; Yamamoto, K.; Otsuka, H.; Takahara, A. Macromolecules 2004, 37, 2203.
29. Wang, W. C.; Neoh, K. G.; Kang, E. T. Macromol Rapid Commun 2006, 27, 1665.
30. Garcia, I.; Tercjak, A.; Zafeiropoulos, N. E.; Stamm, M.; Mondragon, I. J Polym Sci Part A: Polym Chem 2007, 45, 4744.
31. Babu, K.; Dhamodharan, R. Nanoscale Res Lett 2009, 4, 1090.
32. Roth, P. J.; Theato, P. Chem Mater 2008, 20, 1614.
33. Park, J. T.; Seo, J. A.; Ahn, S. H.; Kim, J. H.; Kang, S. W. J Ind Eng Chem 2010, 16, 517.
34. Belegrinou, S.; Malinova, V.; Masciadri, R.; Meie, W. Synth Commun 2010, 40, 3000.
35. Matsuura, K.; Ohno, K.; Kagaya, S.; Kitano, H. Macromol Chem Phys 2007, 208, 862.
36. Xu, F. J.; Neohb, K. G.; Kang, E. T. Prog Polym Sci 2009, 34, 719.
37. Yuan, W.; Yuan, J.; Zhou, L.; Wu, S.; Hong, X. Polymer 2010, 51, 2540.
38. Weaver, J. V. M.; Bannister, I.; Robinson, K. L.; Bories-Azeau, X.; Armes, S. P.; Smallridge, M.; McKenna, P. Macromolecules 2004, 37, 2395.
39. Cadotte, A. J.; DeMarse, T. B. J Neural Eng 2005, 2, 114.